Inorganica Chimica Acta 525 (2021) 120469

Contents lists available at ScienceDirect

Inorganica Chimica Acta

journal homepage: www.elsevier.com/locate/ica

Research paper

A novel coumarin-based pyrazoline fluorescent probe for detection of Fe^{3+} and its application in cells

Ying-Peng Zhang [a,*], Qi Teng [a], Yun-Shang Yang [a,*], Hui-Chen Guo [b], Ji-Jun Xue [c]

[a] School of Petrochemical Engineering, Lanzhou University of Technology, Lanzhou 730050, China
[b] State Key Laboratory of Veterinary Etiological Biology and National Foot and Mouth Disease Reference Laboratory, Lanzhou Veterinary Research Institute, Chinese Academy of Agricultural Sciences, Lanzhou 730046, China
[c] State Key Laboratory of Applied Organic Chemistry & College of Chemistry and Chemical Engineering, Lanzhou University, Lanzhou 730000, China

ARTICLE INFO

Keywords:
Coumarin
Pyrazoline
Fe^{3+}
Fluorescent probe
Cell imaging

ABSTRACT

A novel coumarin-based pyrazoline fluorescent probe A was synthesized through a four-step reaction. The structure was characterized by ^{1}H NMR(Nuclear magnetic resonance), ^{13}C NMR and HR-ESI-MS(High resolution electrospray ionization mass spectrometry). The optical properties of the fluorescent probe was investigated by UV–vis absorption and fluorescence emission spectra. The results showed that the addition of Fe^{3+} makes the fluorescence emission spectra of A quenched and displayed a linear fluorescence response to Fe^{3+} with a detection limit of 1.01×10^{-7} M. It also shows good reversibility upon addition of EDTA(Ethylene diamine tetraacetic acid). The structure of the fluorescent probe was optimized by DFT(Density functional theory) calculations, and the binding mechanism between the fluorescent probe and the recognition ion was explained. Moreover, the probe also has practical application in cell imaging.

1. Introduction

Recently, fluorescent chemosensors for transition metal ions has been attached considerable attentions due to their potential applications in chemical and biological processes [1]. As we know, iron is an essential micronutrient element for most organisms, it plays essential role in oxygen transport and oxygen storage in blood and muscles, and has become an important component of various enzymes and hemoglobin [2]. However, overloaded iron was responsible for cell damage, organ dysfunction and cancer through the abnormal production of reactive oxygen species, hepatitis, Alzheimer's disease [3,4].

Organic small molecule fluorescent probes have the characteristics of low toxicity and high sensitivity, and were widely studied and applied by scientific researchers. Coumarin compound was a lactone compound with benzopyrone structure. Because of its high fluorescence quantum yield, large Stokes shift, good light stability, and easy modification of the structure, its derivatives were widely used in antibacterial, water environment, anti-tumor and other fields [5]. At present, the coumarin-based fluorescent probes mainly include Schiff bases [6–11]and biological thiols [12,13], and there were few reports on coumarin-based pyrazoline fluorescent probes[14,15].

Triphenylamine was a molecule with a central N atom and three benzene rings connected around it to form a star-shaped structure. Because of its special structure, it has larger steric hindrance and higher hole transport rate [16]. Although the fluorescence emission efficiency of triphenylamine was not high, the modified triphenylamine derivatives were used in fluorescent probes [17–20], organic electroluminescent materials [21,23] and organic solar cell materials [24] and other aspects have been widely used. Pyrazoline was widely used in molecular fluorescent probes and other fields due to its excellent blue luminescence properties and strong fluorescence performance [25–33].

Taking all these into account, we have synthesized a new coumarin-based pyrazoline fluorescent probe A. The probe A showed good selectivity to Fe^{3+} over other metal ions. And this probe could be suitable for imaging in living cells.

2. Materials and methods

The raw materials required for the experiment such as triphenylamine, phosphorusvoxychloride, *N*,*N*-dimethylformamide, piperidine, sodium hydroxide, ethanol, and chloroform, Ethyl acetoacetate, 4-(diethylamino) Salicylaldehyde were purchased from commercial channels without further purification. The salts used in stock aqueous solutions of metal ions were KCl, NaCl, $AgNO_3$, $Cu(NO_3)_2$, $HgCl_2$, Mg

* Corresponding authors.
E-mail addresses: yingpengzhang@126.com (Y.-P. Zhang), yangyunshang@tom.com (Y.-S. Yang).

https://doi.org/10.1016/j.ica.2021.120469
Received 24 February 2021; Received in revised form 23 April 2021; Accepted 19 May 2021
Available online 23 May 2021

$(NO_3)_2$, $Ba(NO_3)_2$, $Ca(NO_3)_2$, $CoCl_2$, $Zn(NO_3)_2$, $CdCl_2$, $Fe(NO_3)_3$, $Al(NO_3)_3$, $Fe_2(SO_4)_3$, $FeCl_3$, $Fe(NO_3)_2$, $Ni(NO_3)_2$. ^1H and ^{13}C NMR spectra were recorded on a Avance 400 spectrometer in $CDCl_3$ with TMS as an internal standard. Mass spectrum was recorded on the Thermo Q-Exactive mass spectrometer. The melting point was measured on the XRC-1μ melting point instrument. The ultraviolet absorption was recorded on Cary50. The fluorescence test was recorded on the FE06CN-IF171(ZB) LD/LM luminescence spectrophotometer. The cells were imaged under Leica TCS SP8 MP multiphoton microscopy, HeLa cells was provided by the Lanzhou veterinary research institute, Chinese academy of agricultural sciences.

3. Experimental section

The synthesis route of A was depicted in Scheme 1. Compound 1 and 2 were easily synthesized according to the literature reported methods [34,35]. According to the literature [36], compound 3 was readily prepared from compound 1 and 2 in 65% yield. A mixture of compound 3 (0.5140 g,1.0 mmol) and 85% hydrazine hydrate (0.6123 g, 10.0 mmol) were taken in a 100 mL reaction flask in the presence of glacial acetic acid (15 mL) and refluxed at 118℃ for 7 h. After completion of reaction, it was cooled and poured into crushed ice. The pure product was obtained by silica gel column chromatography (petroleum/ethyl acetate = 1:1) in 60% yield. Melting point(M.p.) 198-202℃. ^1H NMR ($CDCl_3$, 400 MHz) (Fig. S1):δ_H ppm 8.29(s, 1H), 7.35(d, J = 8 Hz, 1H), 7.20(t, J = 12 Hz, 5H), 7.06(t, J = 12 Hz, 5H), 6.98(t, J = 8 Hz, 3H), 6.96 (s, 1H), 6.01(d, J = 8 Hz, 1H), 6.47(s, 1H), 5.51(d, J = 8 Hz, 1H), 3.87 (dd, J = 8, 12 Hz, 1H), 3.44(t, J = 8 Hz, 4H), 2.41(s, 3H), 1.22(t, J = 12 Hz, 7H).^{13}C NMR($CDCl_3$, 100 MHz) (Fig. S2):δ_C ppm 168.56, 160.43, 157.22, 151.70, 146.95, 141.56, 135.96, 129.12, 124.20, 124.06, 122.63, 109.55, 108.44, 96.92, 59.55, 44.98, 44.53, 22.03, 12.46.HR-ESI-MS (Fig. S3) calculated for $[M + H]^+$ 571.2700 , found 571.2703.

4. Results and discussion

4.1. UV–vis absorption of a to Fe^{3+}

In order to explore the selectivity of probe a to different metal cations in THF solution, select Al^{3+}, Ni^{2+}, Ba^{2+}, Co^{2+}, Cd^{2+}, Ca^{2+}, Mg^{2+}, Hg^{2+}, Zn^{2+}, Pb^{2+}, Fe^{2+}, Cu^{2+}, Fe^{3+}, Na^+, Ag^+, K^+ metal ions as the test objects. As shown in Fig. S4, after adding 10 equiv. of the above mentioned ions to the THF solution of probe A, only the addition of Fe^{3+} made the absorption spectrum curve change significantly, the addition of other metal ions did not cause significant changes in the UV–vis absorption spectrum, indicating that the probe A can selectively recognize Fe^{3+}.

4.2. Fluorescence spectra of probe A for selective and anti-interference detection

In order to verify whether the selectivity of probe A in the fluorescence spectrum was consistent with that in the ultraviolet absorption spectrum, use the same buffer solution used in the UV–vis absorption experiment to test its effect on the fluorescence spectrum by adding 10 equiv. of different metal cations. As shown in Fig. 1, the probe A shows a strong fluorescence emission band at 523 nm (fluorescence quantum yield 0.326). When Fe^{3+} was added to the probe A system, the

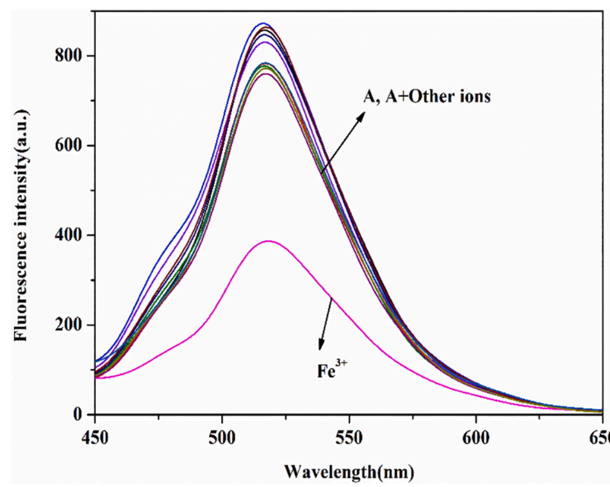

Fig. 1. Fluorescence spectra of probe A(10 μM) in THF solution in the prescence of various metal ions.

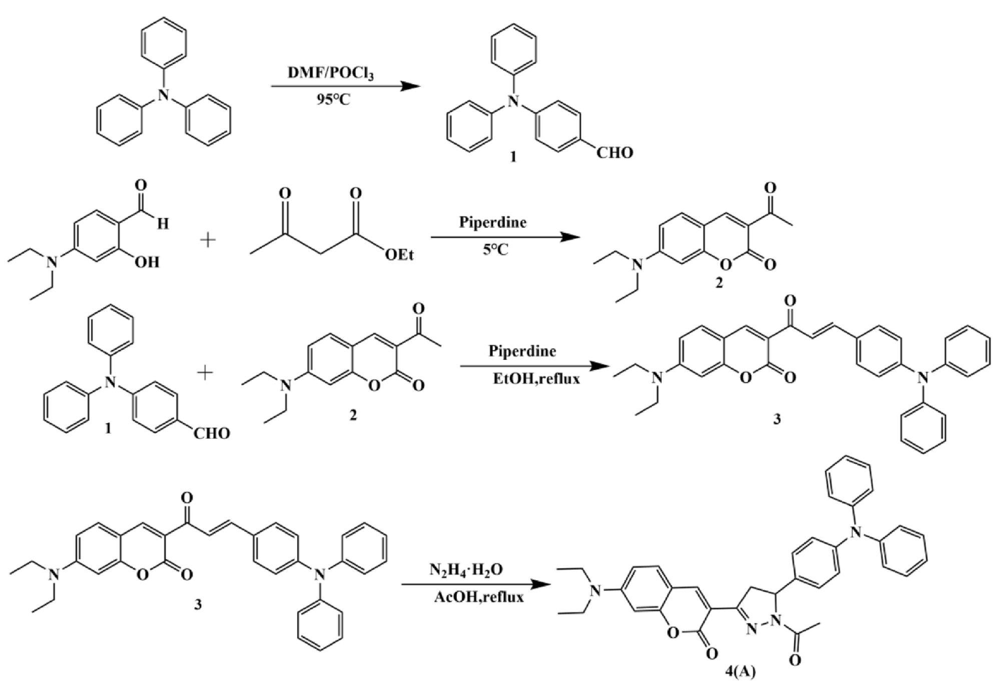

Scheme 1. Synthesis routes of probe A.

fluorescence intensity was quenched to 45%(fluorescence quantum yield 0.108), and the fluorescence quantum yield was calculated by $\Phi = \Phi_s(IA_s/I_sA)(\eta^2/\eta_s^2)$. The addition of Al^{3+}, Ni^{2+}, Ba^{2+}, Co^{2+}, Cd^{2+}, Ca^{2+}, Mg^{2+}, Hg^{2+}, Zn^{2+}, Pb^{2+}, and Fe^{2+}, Cu^{2+}, Na^+, K^+, Ag^+ metal ions did not cause significant changes in the fluorescence spectrum. It shows that probe A has high selectivity to Fe^{3+}.

Meanwhile, considering the interference of other metal cations in practical applications, different metal cations were successively added to the A-Fe^{3+} system to investigate their influence on the fluorescence selectivity. As shown in Fig. 2, the presence of other metal cations failed to cause a significant change in the intensity of the fluorescence spectrum, indicating that the presence of other metal cations will not interfere with the selectivity of probe A.

In order to further explore the selectivity of probe A to Fe^{3+} and its strong anti-interference ability, the fluorescence spectra test was carried out in the presence of iron sulfate, chloride and nitrate in THF solution. It can be seen from Fig. 3 that the fluorescence spectra in the presence of different iron salts have not changed significantly, indicating that the anion will not affect the selective recognition of Fe^{3+} by probe A.

4.3. Titration experiment of probe A to Fe^{3+}

In order to understand the sensitivity of probe A to Fe^{3+}, the fluorescence titration experiment under different Fe^{3+} concentrations was studied. As shown in Fig. 4, with the continuous addition of Fe^{3+}, the fluorescence intensity of probe A gradually decreased. As shown in Fig. 5, a straight line was obtained by the Benesi-Hildebrand equation fitting. It can be found that the binding constant of A- Fe^{3+} complex was 3.5×10^3 M^{-1}, and the detection limit was 1.01×10^{-7} M calculated using 3σ/Ka [37].

4.4. Binding of probe A with Fe^{3+}

In order to study the stoichiometry of probe A and Fe^{3+}, the job's plot experiment was carried out in THF solution. Keeping the total concentration of probe A and Fe^{3+} for 10 μM, and the concentration ratio of 1:9, 2:8, 3:7, 4:6, 5:5, 6:4, 7:3, 8:2 and 9:1 between probe A and Fe^{3+} was titrated [38]. As shown in Fig. 6, the maximum mole fraction of A appears at 0.5, which supporting a 1:1(A: Fe^{3+}) binding stoichiometry. Fig. 7.

In order to fully understand the response of probe A to Fe^{3+}, EDTA was added to the A-Fe^{3+} complex to investigate its influence on the fluorescence intensity. With the addition of EDTA into the A-Fe^{3+} complex, the fluorescence intensity was basically restored. It shows that the complexation between probe A and Fe^{3+} was reversible.

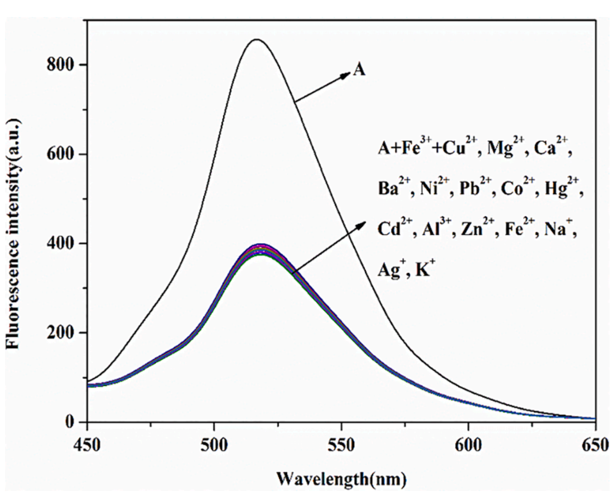

Fig. 2. Fluorescence spectra of probe A(10 μM) and Fe^{3+}(10 equiv.) in the prescence of various metal ions in THF solution.

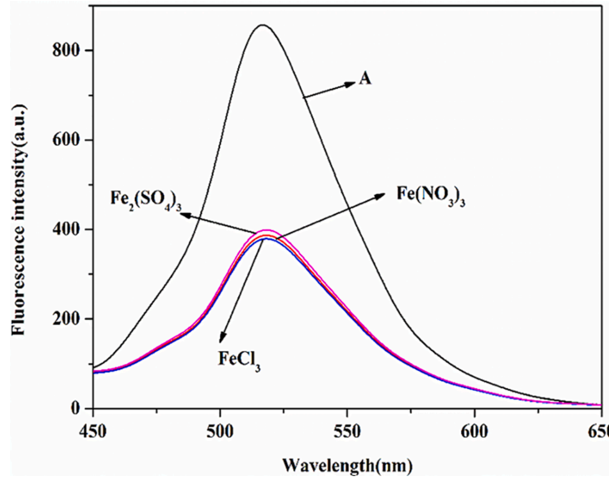

Fig. 3. Fluorescence spectra of probe A(10 μM) in the prescence of different iron salts in THF solution.

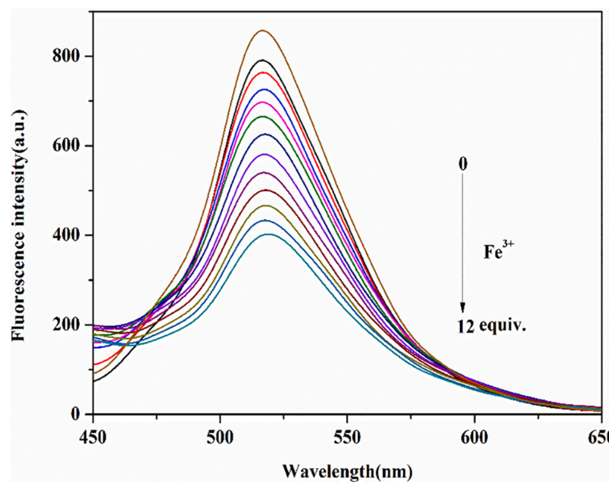

Fig. 4. Fluorescence emission spectra of probe A was titrated with Fe^{3+} (0–12 equiv.) in THF solution.

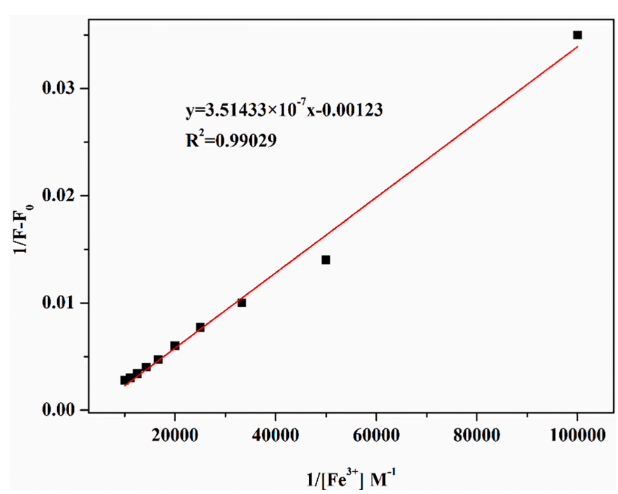

Fig. 5. Benesi-Hildebrand plot of A (10 μM) in THF solution in the presence of Fe^{3+} (0–12 equiv.).

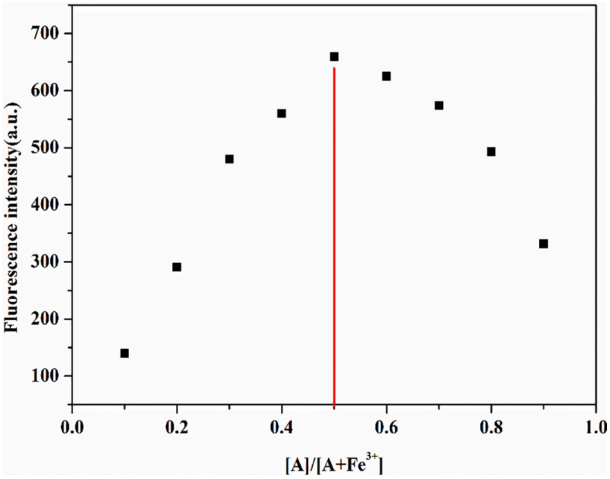

Fig. 6. Job's plot for A with Fe^{3+} in THF solution.

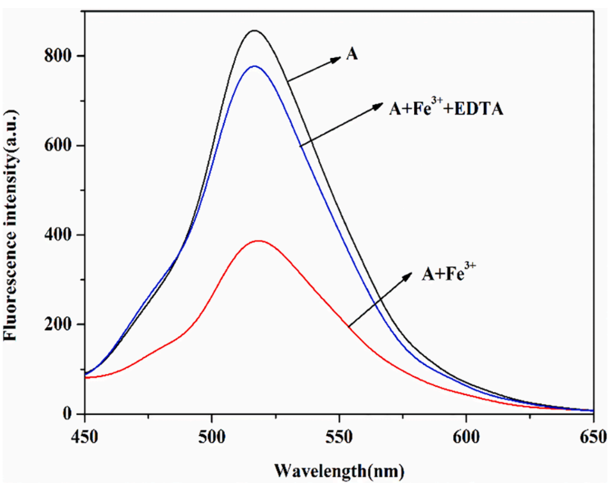

Fig. 7. Reversible study of A to Fe^{3+} with EDTA.

4.5. Cytotoxicity of the probe A

In order to study the biocompatibility of the probe, the MTS method was used to detect the toxicity of probe A to HeLa cells [39]. As shown in Fig. 8, HeLa cells were incubated with 5, 10, 25, 50, and 100 μL probe A,

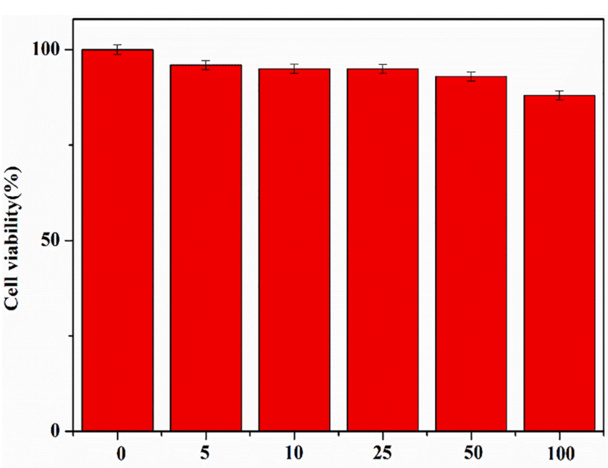

Fig. 8. Cytotoxicity of the probe A in HeLa cells.

respectively. After 24 h, the cell proliferation did not change significantly, and the cell survival rate was greater than 85%. These data indicate that probe A has very low toxicity.

4.6. Imaging of intracellular Fe^{3+}

In order to study the application of probe A in the biological field, fluorescence microscopy imaging technology was used to study its fluorescence imaging in HeLa cells. As shown in Fig. 9, the cells remain intact in the bright field, and green fluorescence appears in the fluorescence field. When the bright field and the fluorescent field overlap, it indicates that the probe A has good cell permeability and can enter the cell. When Fe^{3+} was added to the above system, the fluorescence intensity of probe A in the cell decreased. Therefore, the fluorescence intensity signal of the probe can be used to detect Fe^{3+} in the cell. It also provides a possible method for detecting Fe^{3+} in biological systems in the future.

4.7. Proposed mechanism of A to Fe^{3+}

As shown in Fig. S5, the absorption peak at 1699 cm^{-1} was the characteristic absorption peak of the carbonyl group of α-pyrone. The absorption peak at 1667 cm^{-1} was the characteristic absorption peak of the benzene ring in the coumarin matrix, and the absorption peak at 1621 cm^{-1} was the characteristic absorption peak of the double bond conjugated with the α-pyrone carbonyl group.

The characteristic absorption peak of the carbonyl group in the acetyl group attached to the pyrazole ring was at 1586 cm^{-1}. The absorption peak around 1260 cm^{-1} to 1280 cm^{-1} was the characteristic absorption peak of the C—O bond connected to the carbonyl group of α-pyrone. The absorption peak at 1511 cm^{-1} was the characteristic absorption peak of the C=N double bond on the pyrazole ring.

After adding Fe^{3+}, the characteristic absorption peak of the carbonyl group of α-pyrone shifted from 1699 cm^{-1} to 1738 cm^{-1}, and the characteristic absorption peak of the carbonyl group in the acetyl group connected to the pyrazole ring shifted from 1586 cm^{-1} to 1589 cm^{-1}. The characteristic absorption peak of the C=N double bond on the pyrazole ring shifted from 1511 cm^{-1} to 1515 cm^{-1}. It shows that Fe^{3+} coordinated with probe A at three positions, which changed the characteristic absorption peak wavenumber.

4.8. DFT calculation

Combined with the results of infrared spectroscopy, B3LYP/6–31(G) d and B3LYP/LANL2DZ were used to optimize the structure of probe A before and after the ion was added [40]. As shown in Fig. 10, before ion was added, the electron cloud with the highest molecular orbital of probe A was mainly distributed in the triphenylamine part. The electron cloud with the lowest unoccupied molecular orbital was mainly distributed in the coumarin and pyrazole ring part. After adding Fe^{3+}, the electron cloud distribution has changed. And the energy level difference of the orbital was reduced from 3.3945 eV to 1.1291 eV. It shows that the addition of Fe^{3+} makes the system stable.

4.9. Speculated mechanism of fluorescence

In order to further understand the binding behavior of probe A and Fe^{3+}, ^{1}H NMR titration experiment was studied (Fig. S6). Through experiments, it was found that due to the paramagnetic influence of Fe^{3+}, it has caused serious interference to the peak shape of the compound. However, it can be seen from the figure that the hydrogen protons on the C—N bond on the pyrazole ring (5.40–5.43 ppm) and the hydrogen protons on the $-CH_3$ on the acetyl group (2.27 ppm) have slightly moved. As shown in Scheme 2, according to the results of infrared titration and DFT, it was speculated that the carbonyl group of benzopyrone in the probe A molecule, CH = N and C=O on the pyrazole ring

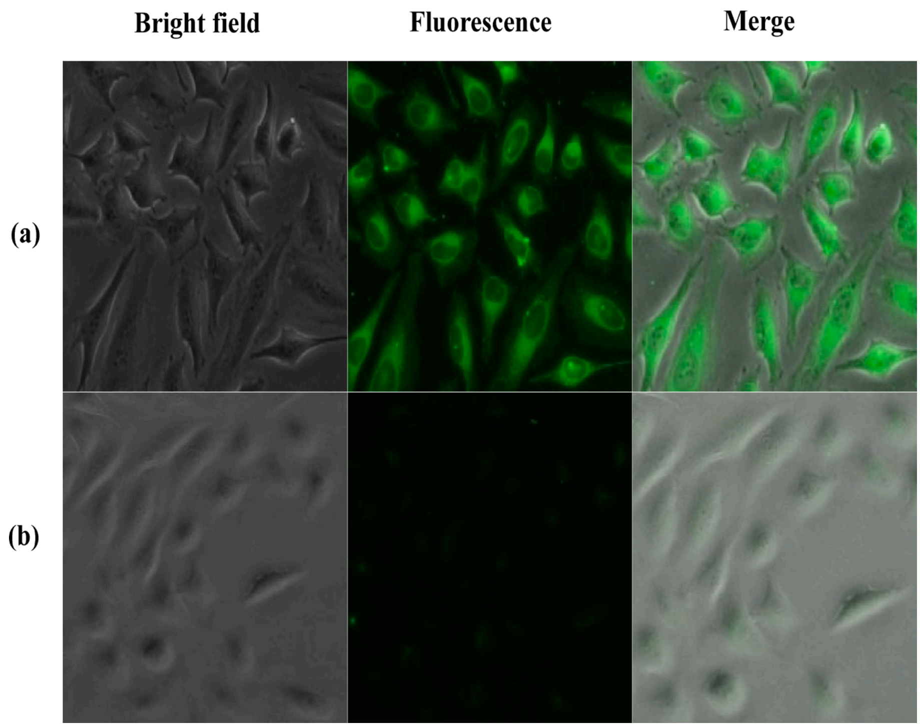

Fig. 9. Fluorescence images of HeLa cells. (a) fluorescence images of HeLa cells incubated with probe A(10 μM); (b) fluorescence images after prescence of Fe^{3+}(100 μM).

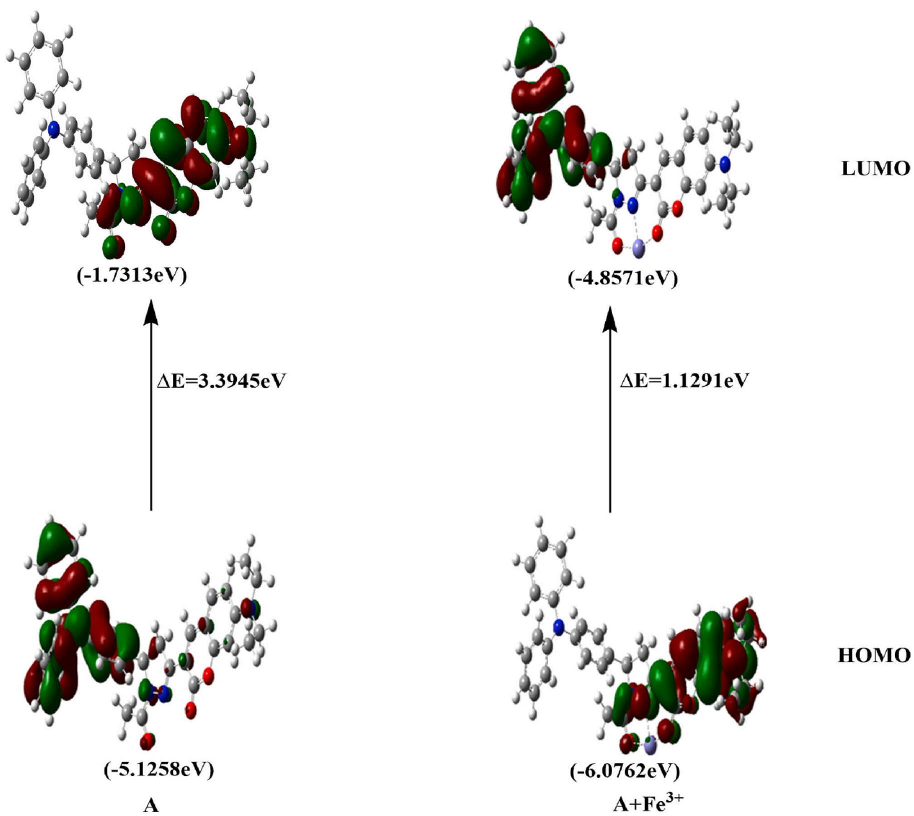

Fig. 10. The HOMO-LUMO energy gaps for probe A and A-Fe^{3+}.

were involved in the coordination of Fe^{3+} in a 1:1 mode. It was because of the coordination of Fe^{3+} that the charge or energy in the molecule was transferred and the fluorescence intensity decreased.

5. Conclusion

In summary, we have designed a novel coumarin-based fluorescent probe A as an analytical tool for detecting Fe^{3+}. The fluorescence was

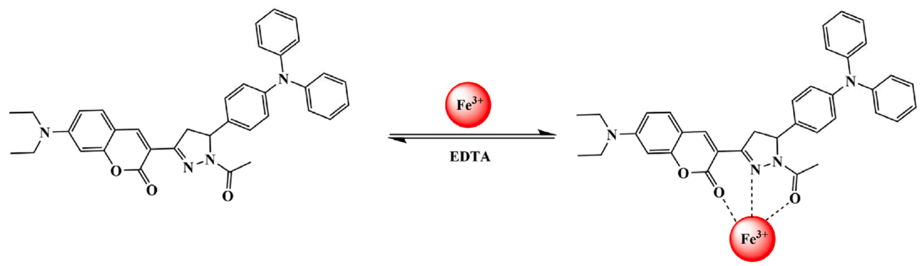

Scheme 2. Proposed binding mode of A with Fe^{3+}.

quenched when Fe^{3+} was added. And the complex process was reversible with Fe^{3+}. The probe A has low toxicity and outstanding cell permeation, which laid the foundation for practical application for fluorescence detection.

CRediT authorship contribution statement

Ying-Peng Zhang: Conceptualization, Methodology, Supervision. **Qi Teng:** Data curation, Writing - original draft. **Yun-Shang Yang:** Investigation, Writing - review & editing. **Hui-Chen Guo:** Data curation. **Ji-Jun Xue:** Software, Validation.

Declaration of Competing Interest

The authors declare that they have no known competing financial interests or personal relationships that could have appeared to influence the work reported in this paper.

Appendix A. Supplementary data

Supplementary data to this article can be found online at https://doi.org/10.1016/j.ica.2021.120469.

References

[1] H. Wang, B. Fang, L. Zhou, D. Li, L. Kong, K. Uvdal, Z. Hu, A reversible and highly selective two-photon fluorescent "on–off–on" probe for biological Cu2+ detection, Org. Biomol. Chem. 16 (2018) 2264–2268.

[2] X. Zhang, Z. Gou, Y. Zuo, W. Lin, A novel polythioether-based rhodamine B fluorescent probe via successive click reaction and its application in iron ion detection and cell imaging, Spectroc. Acta Part A-Molec. Biomolec. Spectr. 228 (2020), 117679.

[3] G. Sathiyan, S. Chatterjee, P. Sen, A. Garg, R.K. Gupta, A. Singh, Thiazolothiazole-Based Fluorescence Probe towards Detection of Copper and Iron Ions through Formation of Radical Cations, ChemistrySelect. 4 (2019) 11718–11725.

[4] H. Chen, J. Huang, B. Hao, B. Yang, S. Chen, G. Yang, J. Xu, Citrate-based Fluorophore-Modified Cellulose Nanocrystals as A Biocompatible Fluorescent Probe for Detecting Ferric Ions and Intracellular Imaging, Carbohydrate Polymers. 224 (2019), 115198.

[5] X.-Y. Sun, T. Liu, J. Sun, X.-J. Wang, Synthesis and application of coumarin fluorescence probes, RSC Adv. 10 (2020) 10826–10847.

[6] K. Wang, P. Sun, X. Chao, D. Cao, Z. Mao, Z. Liu, A coumarin Schiff's base two-photon fluorescent probe for hypochlorite in living cells and zebrafish, RSC Adv. 8 (2018) 6904–6909.

[7] L. Yan, C. Hu, J. Li, A fluorescence turn-on probe for rapid monitoring of hypochlorite based on coumarin Schiff base, Anal. Bioanal. Chem. 410 (2018) 7457–7464.

[8] G. He, X. Hua, N. Yang, L. Li, J. Xu, L. Yang, Q. Wang, L. Ji, Synthesis and application of a "turn on" fluorescent probe for glutathione based on a copper complex of coumarin hydrazide Schiff base derivative, Bioorg. Chem. 91 (2019), 103176.

[9] S. Li, D. Cao, X. Meng, Z. Hu, Z. Li, C. Yuan, T. Zhou, X. Han, W. Ma, A novel schiff base fluorescent probe based on coumarin and benzothiazole for sequential detection of Al^{3+} and PPi and its applicability in live cell imaging, Photochem. Photobiol. A Chem. 392 (2020) 12427.

[10] C. Lin, M. Zhang, X. Yan, R. Zhang, X. He, Y. Yuan, A Coumarin-boronic Based Fluorescent "ON-OFF" Probe for Hg^{2+} in Aqueous Solution, Zeitschrift für anorganische und allgemeine Chemie. 646 (2020) 1892–1899.

[11] L. Zhu, X. Yang, X. Luo, B. Hu, W. Huang, A highly selective fluorescent probe based on coumarin and pyrimidine hydrazide for Cu^{2+} ion detection, Inorg. Chem. Commun. 114 (2020), 107823.

[12] S. Yatong, S. Yanyan, S. Ning, L. Zhipeng, W. Xiangwen, G. Ruifang, C. Duxia, Z. Songfang, Z. Xun, Cyanide and biothiols recognition properties of a coumarin chalcone compound as red fluorescent probe, Spectrochim Acta Part A Mol. Biomol. Spectrosc. 205 (2018) 514–519.

[13] N.K. Hien, M.V. Bay, P.D. Tran, N.T. Khanh, N.D. Luyen, Q.V. Vo, D.U. Van, P. C. Nam, D.T. Quang, A coumarin derivative-Cu^{2+} complex-based fluorescent chemosensor for detection of biothiols, RSC Adv. 10 (2020) 36265–36274.

[14] Y. Hua, Q. Wei, G. Wu, Z.B. Sun, Y.J. Shang, Fluorescent determination of calcium ion using a coumarinyl pyrazoline scaffold and its application in living cells, Anal. Lett. 53 (2020) 960–972.

[15] X. Dai, T. Zhang, Y.Z. Liu, T. Yan, Y. Li, J.Y. Miao, B.X. Zhao, A ratiometric fluorescent probe for cysteine and its application in living cells, Sensors Actuators, B Chem. 207 (2015) 872–877.

[16] H. Zhang, Y. Qu, Y. Gao, J. Hua, J. Li, B. Li, A red fluorescent 'turn-on' chemosensor for Hg^{2+} based on triphenylamine–triazines derivatives with aggregation-induced emission characteristics, Tetrahedron Lett. 54 (2013) 909–912.

[17] B. Dumat, E. Faurel-Paul, P. Fornarelli, N. Saettel, G. Metgé, C. Fiorini Debuisschert, F. Charra, F. Mahuteau-Betzer, M.P. Teulade-Fichou, Influence of the oxazole ring connection on the fluorescence of oxazoyl-triphenylamine biphotonic DNA probes, Org. biomol. chem. 14 (2016) 358–370.

[18] Q. Li, Z. Wang, W. Song, H. Ma, J. Dong, Y.Y. Quan, X. Ye, Z.S. Huang, A novel D-π-A triphenylamine-based turn-on colorimetric and ratiometric fluorescence probe for cyanide detection, Dyes Pigments. 161 (2019) 389–395.

[19] X. Wang, G. Ding, Y. Duan, Y. Zhu, G. Zhu, M. Wang, X. Li, Y. Zhang, X. Qin, C. H. Hung, A novel triphenylamine-based bis-Schiff bases fluorophores with AIE-Activity as the hydrazine fluorescence turn-off probes and cell imaging in live cells, Talanta. 217 (2020), 121029.

[20] B. Liu, Y. Tan, Q. Hu, Y. Wang, X. Wu, Q. Huang, W. Zhang, M. Zheng, H. Wang, A naked eye fluorescent chemosensor for Zn^{2+} based on triphenylamine derivative and its bioimaging in live cells, Chem. Pap. 73 (2019) 3123–3134.

[21] K.J. Thomas, A. Venkateswararao, V. Joseph, S. Kumar, J.H. Jou, Polarity tuning of fluorene derivatives by chromophores to achieve efficient blue electroluminescent materials, Org. Electron. 64 (2018) 266–273.

[22] A. Liang, S. Hu, Z. Wang, W. Zhou, J. Xu, M. Cai, D. Ma, Dibenzothiophene-S, S-dioxide derivatives containing triphenylamine and tetraphenylethene: Synthesis, aggregation-induced emission and electroluminescence, Dyes Pigments. 180 (2020), 108526.

[23] D. Sęk, S. Kotowicz, S. Kula, M. Siwy, A. Szłapa-Kula, J.G. Małecki, S. Maćkowski, E. Schab-Balcerzak, Thermal, spectroscopic, electrochemical, and electroluminescent characterization of malononitrile derivatives with triphenylamine structure, Spectrochim, Acta Part a-Molecular and Biomolecular Spectrosc. 210 (2019) 136–147.

[24] R. Nakar, A.N. Cho, N. Berton, J. Faure-Vincent, F.T. Van, N.G. Park, B. Schmaltz, Triphenylamine 3,6-carbazole derivative as hole-transporting material for mixed cation perovskite solar cells, Chem. Pap. 72 (2018) 1779–1787.

[25] A. Karuppusamy, R. Arulkumar, P. Kannan, P. Venuvanalingam, Effect of increasing methoxyphenyl substitution on pyrene pyrazoline enduring green light emitting materials, J. Photochem. Photobiol. A Chem. 377 (2019) 247–259.

[26] V. Traven, D. Cheptsov, J. Svetlova, I. Ivanov, C. Cuerva, C. Lodeiro, F. Duarte, S. Dunaev, V. Chernyshev, The role of the intermolecular π··· π interactions in the luminescence behavior of novel coumarin-based pyrazoline materials, Dyes Pigments. 186 (2021), 108942.

[27] A. Karuppusamy, P. Kannan, Bluish green emission from pyrene-pyrazoline containing heterocyclic materials and their electronic properties, J. Lumines. 194 (2018) 718–728.

[28] S.A. Khan, Multi-step synthesis, photophysical and physicochemical investigation of novel pyrazoline a heterocyclic D-π-A chromophore as a fluorescent chemosensor for the detection of Fe^{3+} metal ion, J. Mol. Struct. 1211 (2020), 128084.

[29] M. Rangasamy, K. Palaninathan, Thiophene and furan appended pyrazoline based fluorescent chemosensors for detection of Al^{3+} ion, Inorg. Chem. Commun. 101 (2019) 177–183.

[30] E. Bozkurt, H.I. Gul, E. Mete, Solvent and substituent effect on the photophysical properties of pyrazoline derivatives: A spectroscopic study, J. Photochem. Photobiol. A Chem. 352 (2018) 35–42.

[31] Y. Chen, J. Guo, X. Wu, D. Jia, F. Tong, Color-tuning aggregation-induced emission of o-Carborane-bis (1, 3, 5-triaryl-2-pyrazoline) triads: Preparation and investigation of the photophysics, Dyes Pigments. 148 (2018) 180–188.

[32] M. Rangasamy, K. Palaninathan, A pyrazoline-based fluorescent chemosensor for Al^{3+} ion detection and live cell imaging, New. J. Chem. 42 (2018) 10891–10897.
[33] A. Tigreros, J. Portilla, Recent progress in chemosensors based on pyrazole derivatives, RSC Adv. 10 (2020) 19693.
[34] H. Jin, X. Li, T. Tan, S. Wang, Y. Xiao, J. Tian, Electrochromic properties of novel chalcones containing triphenylamine moiety, Dyes Pigments. 106 (2014) 154–160.
[35] Y. Zhang, Y. Yan, S. Xia, S. Wan, T.E. Steenwinkel, J. Medford, E. Durocher, R. L. Luck, T. Werner, H. Liu, Cell Membrane-Specific Fluorescent Probe Featuring Dual and Aggregation-Induced Emissions, ACS Appl. Mater. Interfaces 12 (2020) 20172–20179.
[36] J. Yin, M. Peng, Y. Ma, R. Guo, W. Lin, Rational design of a lipid-droplet-polarity based fluorescent probe for potential cancer diagnosis, Chem. Commun. 54 (2018) 12093–12096.
[37] X. Xia, Y. Fu, H. Tang, Y. Li, F. Wang, J. Ren, A self-assembled micellar nanoprobe for specific recognition of hydrazine in vitro and in vivo, Sensors Actuator, B Chem. 272 (2018) 479–484.
[38] N. Zhang, X. Tian, J. Zheng, X. Zhang, W. Zhu, Y. Tian, Q. Zhu, H. Zhou, A novel fluorescent probe based on the flexible dipicolylamine: Recognizing zinc (II) in aqueous solution and imaging in living cell, Dyes Pigments. 124 (2016) 174–179.
[39] Y.P. Zhang, Q.H. Xue, Y.S. Yang, X.Y. Liu, C.M. Ma, J.X. Ru, H.C. Guo, A chromene pyrazoline derivatives fluorescent probe for Zn^{2+} detection in aqueous solution and living cells, Inorganica. Chim. Acta. 479 (2018) 128–134.
[40] S. Lal, S. Kumar, S. Hooda, P. Kumar, A highly selective sensor for Cu^{2+} and Fe^{3+} ions in aqueous medium: Spectroscopic, computational and cell imaging studies, J. Photochem. Photobiol. A Chem. 364 (2018) 811–818.